Process Safety and Environmental Protection 153 (2021) 167–177

Contents lists available at ScienceDirect

Process Safety and Environmental Protection

journal homepage: www.elsevier.com/locate/psep

Pipeline leak detection based on variational mode decomposition and support vector machine using an interior spherical detector

Tianshu Xu[a,b], Zhoumo Zeng[a,b], Xinjing Huang[a,b,*], Jian Li[a,b], Hao Feng[a,b]

[a] State Key Laboratory of Precision Measuring Technology and Instruments, Tianjin University, Tianjin 300072, China
[b] Binhai International Advanced Structural Integrity Research Centre, Tianjin 300072, China

ARTICLE INFO

Article history:
Received 25 March 2021
Received in revised form 11 June 2021
Accepted 14 July 2021
Available online 16 July 2021

Keywords:
Pipeline
Leak detection
Spherical detector
Signal de-noising

ABSTRACT

A spherical detector (SD) is capable of closely approaching a leak point and collecting leak sounds from the inside of a long pipeline, thereby enabling an extremely high leak detection sensitivity. However, acoustic noises arise from collision and friction while the SD is rolling forward, hindering the identification of leak acoustic signals. To address this challenge, this work presents a pipeline leak identification method for an SD based on combining variational mode decomposition (VMD) and a support vector machine (SVM). A leak generation system is set up where the pipe is water-filled, pressurized, and tiltable, and the SD can stand still or roll to collect a sufficient variety of leak sound samples. By decomposing the noisy signals into different modes and selecting the modes with high correlations to reconstruct the signals, the VMD can significantly decrease the collision noise. Additionally, the Mel frequency cepstral coefficients (MFCCs) are extracted and used to constitute a characteristic vector for SVM-based leak recognition. The trained neural network effectively identifies the occurrence of a leak; the recognition accuracy can reach up to 93 %, with a satisfactory specificity of 89.6 %.

1. Introduction

Pipelines are widely used to transport fluids over a long distance, and are generally found in water distribution systems (WDSs) and the petrochemical industry. However, pipelines are susceptible to leakage owing to pipe defects, such as corrosion, fatigue cracks, and dents (Xie and Tian, 2018). Leak accidents not only influence people's normal lives, but can also lead to massive economic losses and ecological disasters. Therefore, effective leak detection methods for pipelines have become a top priority.

Commonly, leak detection techniques can be classified based on whether the detection is conducted inside or outside the pipeline (Waleed et al., 2019). Among all of the present solutions, acoustic detection techniques have distinguished themselves owing to their advantages in regards to a higher sensitivity, better location accuracy, lower false alarm rate, faster response time, and higher adaptability (Liu et al., 2017). Acoustic leak-detection techniques can be implemented in the form of both external and internal detection, via identifying the sounds or vibrations induced by liquid escaping from pipes under pressure.

When a leak occurs, acoustic signals are generated owing to fluid turbulence (Papastefanou et al., 2012). The leak-induced acoustic signals propagate upstream and downstream along both the pipeline wall and liquid column inside, and can be ultimately captured by accelerometers or hydrophones at the two ends of the pipeline. A cross-correlation analysis is then employed to calculate the arrival time difference of the acoustic signals propagating to the pipeline ends; accordingly, the leak position can be determined.

Many efforts have been made in both physics modeling and signal processing to improve this type of dual-sensor-based method. Muggleton et al. studied the wavenumber of waves in a buried pipe to calculate the propagation wave speeds and wave attenuation (Muggleton et al., 2002). Gao et al. introduced an analytical model for a cross-correlation function for wave propagation in buried plastic pipes, and studied the effect of band-pass filtering on leak detection (Gao et al., 2004). Liu et al. studied a propagation model for leakage acoustic waves in natural gas pipelines (Cui-wei et al., 2015). Xu et al. used a wavelet packet transform de-noising method to improve leak identification performance (Xu et al., 2013).

The inherent drawback of using the acoustic waves propagating along a pipeline to detect a leak is that the detection distance is very short, owing to severe acoustic attenuation (Liu et al., 2003; Hunaidi and Chu, 1999). An alternative method is to use a negative pressure wave (NPW) to monitor the leak; the NPW is a type of infrasound capable of propagating tens of kilometers (Chun-hua et al., 2012).

* Corresponding author at: State Key Laboratory of Precision Measuring Technology and Instruments, Tianjin University, Tianjin 300072, China.
E-mail address: huangxinjing@tju.edu.cn (X. Huang).

https://doi.org/10.1016/j.psep.2021.07.024
0957-5820/

An improved NPW algorithm was recently introduced in which the attenuation was used instead of the time difference, allowing for a more precise location of the pipe leak. However, an NPW-based method can only detect sudden leaks representing greater than 1 % of the pipeline output, i.e., massive leaks. In contrast, continuous small leaks cannot generate NPWs (Li et al., 2019). Another alternative method is to use distributed optic fibers to monitor the vibration or temperature changes caused by a leak in real time (Jingyi et al., 2017). However, the optic fibers must be simultaneously built with the pipeline, and most of the old pipelines with high leak risks have no accompanying optic fibers. In addition, the complex coupling between the surrounding medium and pipeline may introduce severe distortions to NPWs and/or significantly interfere with an optic fiber sense system (Gao et al., 2017; Brennan et al., 2017).

To overcome the leak detection limitations of external methods, various in-pipe inspection techniques have been proposed, e.g., by launching a sound sensor into a pipeline to get close to a leak point for a highly sensitive detection and accurate localization of leaks. A tethered water leak detector named Šaharaẅas developed (Laven et al., 2006); in this system, a leak signal could be sent back to a host computer in real time with a tethered cable. The detector was tracked using an above-ground marker, and was applicable to pipelines with a diameter of more than 300 mm. The detection sensitivity could reach up to 0.02 L/min. Another proposed universal in-pipe structural health monitoring system uses a pipeline inspection gauge (PIG) (Tandon, 1997). The PIG is pushed forward by the oil flow, and is equipped with a wide variety of sensors (i.e., not limited to acoustic sensors). It can perform different tasks, such as leak detection, crack detection, metal loss detection, and pipeline geometry detection. An ultrasonic method was used to detect cracks in (Jaesun et al., 2018), but the pipe wall needed to be closely fitted to send and receive signals. In general, the material of a pipe is usually metal, and the above methods are not applicable to plastic pipes. Moreover, although the PIG is commonly used in oil pipelines, and it is barely used in WDSs, owing to its extremely complicated operating procedures and easy blockage of the pipeline. Recently, researchers have studied a spherical detector (SD) for leaks, i.e., a detector that can freely roll within pipes (Xu et al., 2019; Kumar et al., 2017a; Kumar et al., 2017b).

The diameter of the SD is smaller than that of the pipeline, allowing it to easily pass through the pipeline under the push of the water or oil flow. After special design, the SD can pass through a vertical pipe (Guo et al., 2014); thus, it can be applied to different liquid pipelines without being limited by the surroundings. Moreover, the SD is immune to the influence of many external factors, such as the pipe materials and surrounding medium. The SD is equipped with acoustic sensors with high sensitivity to capture acoustic signals as they travel inside and along the pipeline. After the entire inspection is completed, the data are uploaded to the host computer for processing and analysis.

When the SD rolls in the pipeline, the sounds caused by collision and friction between the SD and pipe wall may contaminate the leak-induced sound, hindering the identification of tiny leaks. Studies based on acoustic detections have reported that the leak-induced acoustic signals in the liquid column are mostly in the low-frequency band, usually below 10 kHz (Hunaidi and Chu, 1999; Mostafapour and Davoudi, 2013; Jinghui et al., 2019). Our recent experiment (using a mobile SD to implement acoustic leak detection) also confirmed this point, and further indicated that the frequency spectrum of the leak signal may overlap with that of the collision and friction sound. This may lead to missing and false leak detection.

However, relatively few studies have considered the de-noising of acoustic leak signals detected by an SD. Advanced signal denoising and feature extraction algorithms are required to improve the leak detection rates of SDs. Given that the interference signals caused by rolling are non-stationary, an appropriate de-noising method should be applied to extract the signal characteristics (Mengfei et al., 2019). A filter-based noise reduction method is a traditional tool to deal with steady noise; however, it cannot perform well in terms of non-stationary and transient signals (Basu and RoyChaudhuri, 2016). A wavelet threshold de-noising method has gained widespread attention, owing to its advancement in multi-resolution analysis (Zhong et al., 2016; Ahadi and Bakhtiar, 2010). Nevertheless, the selection of the wavelet base function and threshold significantly influences the final results. Empirical mode decomposition (EMD) (Huang et al., 1998) is an adaptive time-frequency processing method for managing non-stationary signals, and has recently been used for pipeline leak detection (Sun and Wen, 2013; Li et al., 2014). However, EMD has some drawbacks, including mode mixing and inadequate enveloping (Tang et al., 2012).

In this work, variational mode decomposition (VMD) is employed to separate leak signals from interference signals. As a state-of-the-art non-recursive and self-adaptive signal-processing algorithm, VMD can effectively decompose non-stationary and non-linear signals into several bandwidth-limited elements called intrinsic mode functions (IMFs) (Dragomiretskiy and Zosso, 2014). First, the acoustic signals from the SD are collected and decomposed into a list of IMFs. The IMFs containing leak information are selected to reconstruct the denoised signal by calculating the correlation coefficient between each IMF and reference signal. Second, feature vectors are extracted based on the Mel-frequency cepstral coefficients (MFCCs). Finally, a support vector machine (SVM), a generalized linear classifier, is used to distinguish the leak cases.

The remainder of this paper is organized as follows. Section 2 briefly presents the theoretical foundations of VMD and MFCCs. The experimental setup and denoising algorithm are described in Section 3. Section 4 presents the feature extraction method and SVM classifier for leak identification. Finally, the conclusions are summarized in Section 5.

2. Methodology

2.1. Variational mode decomposition (VMD)

The purpose of VMD is to decompose an input real-valued signal g into a discrete number of modes called IMFs, where each mode has a limited bandwidth and an estimated center frequency. The construction and solution of VMD is considered as a constrained variational optimization problem, described as follows:

$$\begin{cases} \min\limits_{\{u_k\},\{\omega_k\}} \left\{ \sum\limits_{k=1}^{K} \left| \left| \partial_t [(\delta(t) + \frac{j}{\pi t}) * u_k(t)] e^{-j\omega_k t} \right|_2^2 \right\} \\ s.t. \sum\limits_{k=1}^{K} u_k = g \end{cases} \tag{1}$$

In the above, μ_k and ω_k represent the sets of all modes and corresponding center frequencies, respectively; K is the decomposition mode number; and $\delta(t)$ represents the Diarc distribution.

To solve (1), the Lagrangian multiplier λ and quadratic penalty term α are used to make the problem unconstrained. Herein, λ can enhance the constrained stringency, whereas α can effectively

guarantee the reconstructed accuracy. The augmented Lagrangian is determined as follows:

$$L\left\{\left\{u_k\right\},\left\{\omega_k\right\},\lambda\right\} = \alpha\sum_k \left\| \partial_t \left[\left(\delta(t)+\frac{j}{\pi t}\right) * u_k(t) \right] e^{-j\omega_k t} \right\|_2^2 + \left\| g(t) - \sum_k u_k(t) \right\|_2^2 + \left\langle \lambda(t), g(t) - \sum_k u_k(t) \right\rangle \quad (2)$$

Thus, the solution of (1) is transformed into finding the saddle point of (2). The alternate direction method of multipliers is applied to obtain the saddle point. The optimal is directly updated using Wiener filtering. The updated μ_k and ω_k are calculated using (3) and (4).

$$\hat{u}_k^{n+1} = \frac{\hat{g}(\omega) - \sum_{i\neq k}\hat{u}_i(\omega) + \frac{\hat{\lambda}(\omega)}{2}}{1+2\alpha(\omega-\omega_k)^2} \quad (3)$$

$$\omega_k^{n+1} = \frac{\int_0^\infty \omega \left|\hat{u}_k(\omega)\right|^2 d\omega}{\int_0^\infty \left|\hat{u}_k(\omega)\right|^2 d\omega} \quad (4)$$

After the modes and center frequencies are acquired, the Lagrangian multipliers are renewed as follows:

$$\hat{\lambda}^{n+1} = \hat{\lambda}^n + \tau\left(\hat{g} - \sum_k \hat{u}_k^{n+1}\right) \quad (5)$$

Here, τ is an updated factor, and represents the noise tolerance. Finally, the above iteration of (3)–(5) is completed until the rule in (6) is satisfied.

$$\sum_k \left(\left\| \hat{u}_k^{n+1} - \hat{u}_k^n \right\|_2^2 / \left\| \hat{u}_k^n \right\|_2^2 \right) < \varepsilon \quad (6)$$

After these steps, the original signal is decomposed into K narrow-band IMF components.

2.2. Mel frequency cepstral coefficients (MFCCs)

MFCCs (Davis and Mermelstein, 1980) represent the power spectrum distribution of an acoustic signal, and are based on the non-linear Mel scale of frequency. MFCCs have been the dominant features used for automatic speech recognition (ASR), owing to their good performance in characterizing the speech spectrum in a compact form. MFCCs are typically derived as follows.

(1) Segment: The acoustic signal is divided into short time frames, generally by moving a window function (Hamming window, for example) at fixed intervals. Each frame is considered as a stationary signal, i.e., the signal remains unchanged during this time.
(2) Fast Fourier transform (FFT): The FFT of each frame is taken to obtain the frequency spectrum.
(3) Map and filter: The spectrum acquired above is mapped onto the Mel scale, as follows:

$$Mel(f_m) = 2595lg(1+f/700) \quad (7)$$

In the above, f is the standard frequency. A bank of L triangular filters with center frequencies uniformly spaced over the Mel frequency is applied to calculate a weighed sum of the filter spectral components; typically, L is 24. The sum of each filtered spectral component constitutes the filter bank energy, m(l).

(4) Discrete cosine transform (DCT):: The DCT of the list of filter-bank energies is considered to obtain the MFCCs.

$$c_{mfcc}(i) = \sqrt{\frac{2}{L}}\sum_{l=1}^{L} lgm(l)\cos\{(l-0.5)\frac{i\pi}{L}\} i = 1, 2, \ldots N \quad (8)$$

2.3. Proposed method

VMD is a new non-recursive decomposition method for managing non-stationary signals, and can decompose complex noise signals into a set of relatively stable IMFs with their own center frequencies. To separate a leak signal from an interference signal, the original non-stationary signal recorded by the SD is decomposed into K modes based on VMD; these are more regular than the original signal. The mode number K is determined based on the center frequency, ω_k. The main frequency band of the leak signal is known from prior knowledge based on a previous study (Tandon, 1997), and the maximum ω_k should not exceed 1.5 × the upper band limit. When K continues to increase, the corresponding ω_k is mostly occupied by noise instead of leak signals. The leak signal measured by microphones is an acoustic signal that is similar to a speech signal. The feature of a speech signal is mainly represented by spectral features such as MFCCs; hence, the leak signal can also be characterized by the MFCCs.

Based on the VMD and SVM, the method proposed in this work for detecting pipeline leaks is conducted in three steps, as follows. A flowchart of the proposed method is presented in Fig. 1.

Step 1: Signal de-nosing.

(1) Collect the original signals measured by the SD;
(2) Determine the decomposition layers based on the center frequencies;
(3) Calculate the correlation coefficients between the original signal and IMFs using VMD, and screen out the noise IMFs with low correlations; and
(4) Reconstruct the useful IMFs.

Step 2: Feature extraction.

Apply the MFCCs to differentiate between leak signals and non-leak signals.

Step 3: SVM-based leak identification.

(1) Divide the de-noised signals into training sets and test sets;
(2) Input the MFCCs of the de-noised signals to execute the training model; and
(3) Obtain the classification results of leak signals with different leak apertures.

3. Experimental investigation of leak signals

Several validation experiments have been conducted on oil pipelines and urban water supply pipes in China, as an SD can work properly therein without requiring the instructions of veteran engineers. Notably, the SD has little impact on the normal operations of pipelines. Therefore, the SD could be a safe approach to providing health monitoring for pipelines.

3.1. Experimental setup

In this study, the experiments were conducted on a 12-m long, Φ219 mm, X52 steel pipe with pressurized water inside; this pipe satisfied the national standard, and the length was sufficiently long

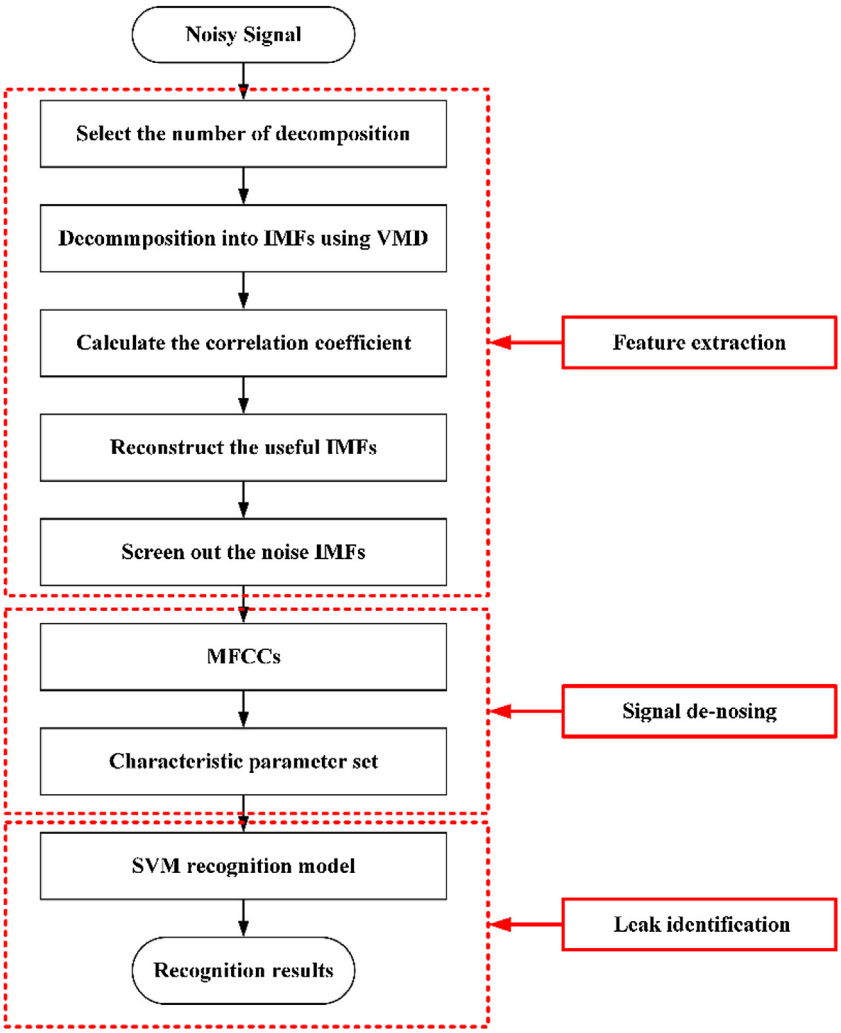

Fig. 1. Procedure of the proposed method for leak detection.

for the leak signal to attenuate from the center to the end. The general layout of the leak detection test system is shown in Fig. 2. The pipe was sealed with two flange plates at each end. The water was pressurized by a booster pump with a maximum pressure of 1.2 MPa (a common pressure in oil pipelines). Round leak holes of different sizes were manufactured on several steel plugs, and the plugs were embedded one-by-one in the middle of the pipe to generate leaks with different leak rates. The SD used in the experiments is shown in Fig. 2(a); its internal layout is shown in Fig. 3. Two digital microphones (SPH0645) from Knowles were used to collect the acoustic signals. The microphone was omnidirectional, with a high signal-to-noise ratio (SNR) of 65 dB. The output rate was 44.1 kHz, and the original signals were recorded on a 32 GB memory card. Based on the Nyquist sampling theorem, the highest frequency resolution was 22.05 kHz, satisfying the requirements for the identification of leak signals. A polyurethane shell was attached onto the SD to enhance the sound transmission and shock absorption capacity. The pump was closed, as the leak signal was recorded to decrease the influence of disturbances from the pump.

Two groups of experiments were conducted. First, the SD was placed still on a ball base immediately below the leak point, as shown in Fig. 2(a), and the leak acoustic signal was acquired as a standard signal with no interference noise caused by collisions between the SD and pipe wall. Second, the SD was freely placed at one end of the pipe and the pipe was tilted by a lifting crane, so that the SD could roll down to the other end of the pipe and pass by the leak point, as shown in Fig. 2(b); this could mimic the field conditions, that is, where the SD rolls forward in a pipeline with a flow.

3.2. Time and frequency domain analysis of leak signals

The standard leak signals measured when the SD was still are shown in Fig. 4(a). During the experiments, the pressure was maintained at 1.0 MPa. Four leak apertures were tested: 1.0 mm, 0.8 mm, 0.6 mm, and 0.4 mm, and the corresponding signals are displayed in Fig. 4(a) from top to bottom. The intensity of the leak signals was scaled by the root mean square (RMS) value of the original signals, as shown in Fig. 4(b). It can be seen that the intensity of the leak signal gradually decreases as the leak aperture decreases. The information acquired from the time domain of the leak signals is limited, so the frequency spectrum is used, as illustrated in Fig. 5. The frequency spectra of the four signals are almost the same; all of them have a main peak at approximately 1615 Hz, and some secondary peaks at approximately 1100 Hz, 2670 Hz, and so on. All of these peaks form the frequency features of the leak signals, and are called the characteristic frequencies (Tandon, 1997). Fig. 6 depicts the envelope spectra of the 1-mm leak signal and non-leak signal; it can be seen that the amplitude of the leak signal drops significantly at approximately 4 kHz, and reaches almost the same level as the non-leak signal. Moreover, no additional peaks with amplitudes larger than 3.8 kHz exist above 4 kHz; that is, most of the energy

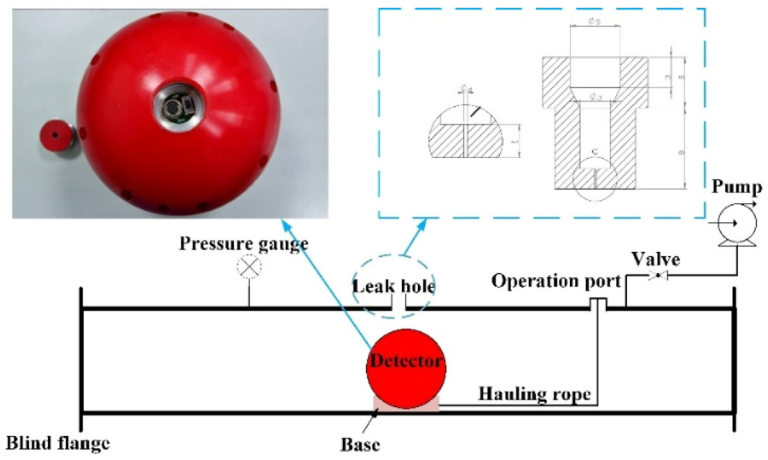

(a)

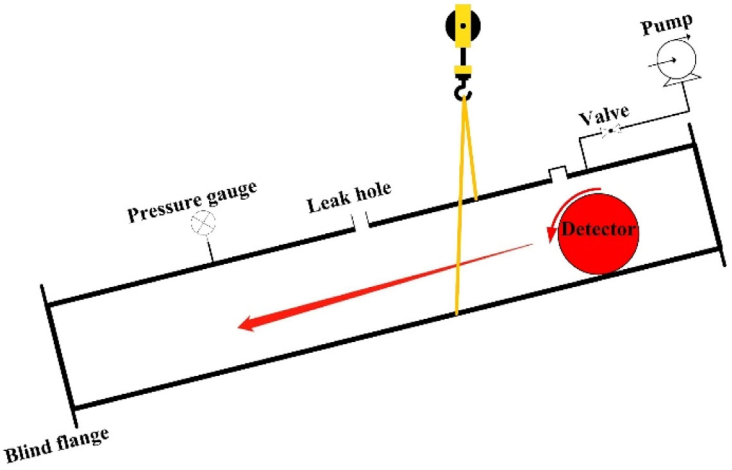

(b)

(c)

Fig. 2. Experiment apparatus and process: (**a**) The spherical detector (SD) used in the experiments and the leak plug dimensions; the SD is still and right below the leak point. (**b**) the SD is rolling down and passing by the leak point. (**c**) Experiment photos.

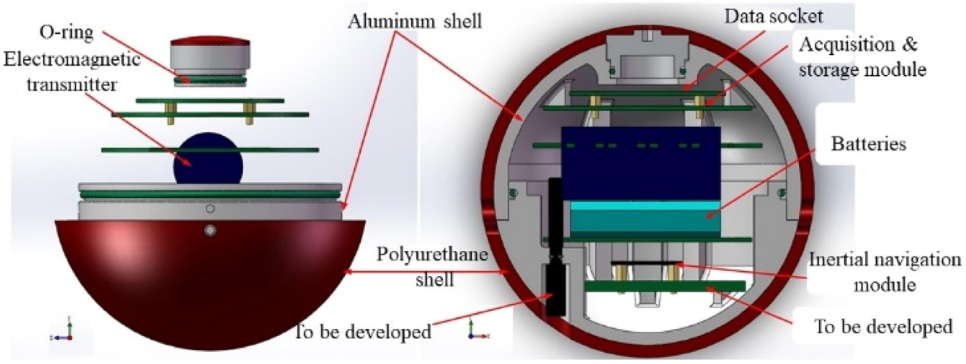

Fig. 3. Internal layouts of the SD.

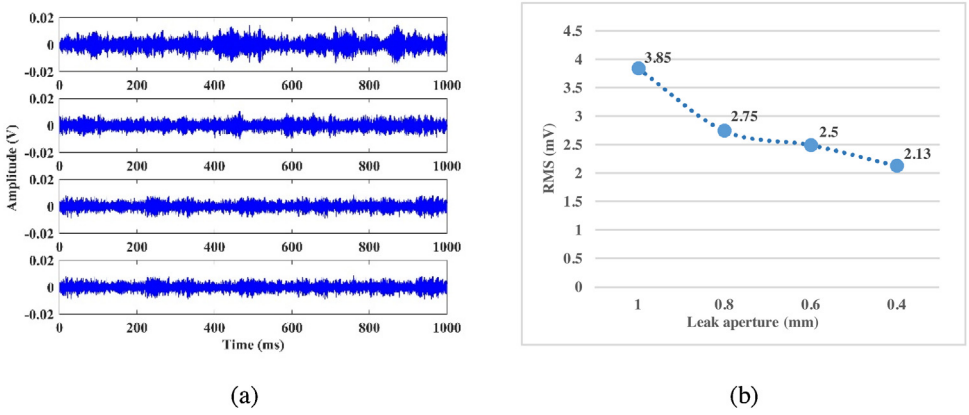

Fig. 4. (**a**) Time domain of leak signals with different leak apertures. (**b**) Root mean square (RMS) of leak signals with different leak apertures.

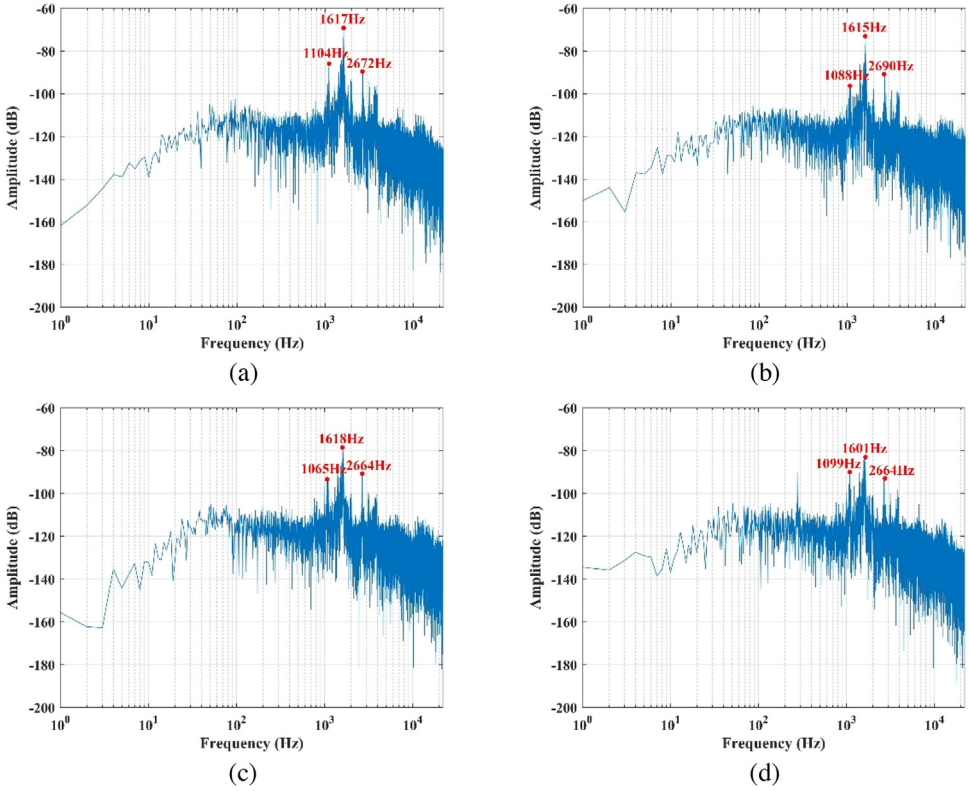

Fig. 5. Frequency spectrums of the leak signals with different leak apertures. (**a**) 1.0 mm. (**b**) 0.8 mm. (**c**) 0.6 mm. (**d**) 0.4 mm.

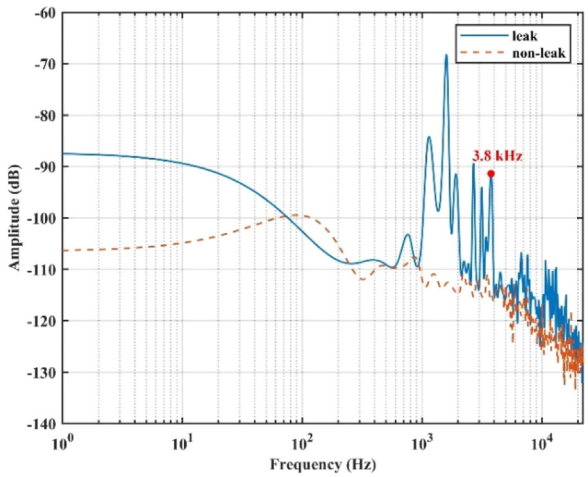

Fig. 6. Envelope spectrums of the leak signal (1 mm) and non-leak signal.

of the leak signal is concentrated in the frequency band below 4 kHz. The time and frequency domain analysis of the leak signals indicates that the leak signals are quite steady when the detector is still; the leak apertures only influence the signal intensity, and do not change the shape of the frequency spectrum.

Then, the leak signal with interference was measured when the detector rolled down from one end of the pipe to the other. Fig. 7(a) and (b) depicts the time-domain signal and its corresponding frequency spectrum using the short-time Fourier transform (STFT). The SD arrives at the center of the leak at 13–15 s, i.e., where the spectrogram has richer components. As the SD moves away from the leak, the intensity of the characteristic frequencies decays. Hence, the frequency bands around these characteristic frequencies can be used to distinguish leaks. However, the frequency bands are easily polluted by the interference noise.

A frame of interfered-with leak signals in the time domain and its corresponding STFT are illustrated in Fig. 8. It can be seen that once the detector rolls along the pipe, the signal is disturbed. The unevenness inside the pipe causes the detector to bump when rolling, leading to unexpected interference noise. As shown in Fig. 8(c) and (d), the different intensities of impulse noise occupy different frequency bands. Noise 1 is so strong that it almost dominates all of the frequency domain from 0 Hz to 20 kHz, whereas noise 2 is much gentler, and is only distributed in the band below 2 kHz. Hence, it is difficult to eliminate interference noise using a normal digital filter.

4. De-noising of leak signals with VMD

VMD was applied to separate the leak signal from the inference signal. A frame of the standard leak signal $x(n)$ was used as a clean reference signal. For a better comparison of the noise reduction effect, a 'pseudo' synthetic leak signal $p(n)$ was used instead of a 'real' measured interfered leak signal. The synthetic signal was composed of a standard leak signal and a rolling interference signal, as follows:

$$p(n) = x(n) + r(n) \tag{9}$$

In the above, $r(n)$ is the rolling signal. This synthetic signal could simulate real leak conditions, and simultaneously contained a reference leak signal for comparison with the de-noised signal. The two signals are shown in Fig. 9.

One of the key factors in VMD is the number of decomposition layers, K. Each layer represents one mode of the signal. Too few modes lead to under-segmentation of the signal, and too many modes either capture extra noise or lead to mode duplication. In this study, the number K was determined according to the center frequency ω_k of each mode. The center frequencies corresponding to different K values ranging from two to five are listed in Table 1. As mentioned above, the energy of the leak signal was mostly concentrated in the frequency band below 4 kHz. When the mode K increased up to 4, the highest center frequency was approximately 14 kHz, which significantly exceeded the frequency range. Hence, K was set as 3.

Table 1
ω_k of each mode according to different K.

K	ω_k /Hz				
	μ_1	μ_2	μ_3	μ_4	μ_5
2	102.7	1167.5			
3	102.1	1132.5	5950.2		
4	102	1131	5792	14,465	
5	101	1083	3691	6496	14,555

Table 2
Correlation coefficients between each decomposition signal (intrinsic mode function (IMF)) and the standard leak signal.

	IMF1	IMF2	IMF3
correlation coefficient	0.1080	0.6175	0.3575

Decomposition with three modes for the synthetic leak signal was performed using the VMD program in MATLAB. The intrinsic modes and their corresponding normalized spectra are shown in Fig. 10. From the figure, we can see that mode 1 inherits most of the interference signal, and its frequency components are mostly distributed in the low-frequency band, specifically below 500 Hz. Compared with Fig. 5, the frequency range of mode 2 is consistent with the leak signal, and is mostly in the range of 700–3000 Hz. The band distribution of mode 3 is approximately 3000–8000 Hz, and the amplitude is apparently lower than those of the other two modes. Both modes 2 and 3 are well maintained from the interference signal. To quantify the noise level of each decomposition signal, the correlation coefficients of the decomposition signals with the standard leak signal are calculated, as shown in Table 2. It can be concluded that mode 1 has the least correlation with the leak signal, whereas mode 2 is the most relevant component in regards to the leak signal. Therefore, IMF 1 is considered as a noise component. This conclusion is consistent with the frequency analysis mentioned above.

The de-noised signal is reconstructed using IMF 2 and IMF 3 without IMF 1, and the results are shown in Fig. 11. It can be seen when comparing Figs. 9b and 11 b that the noises after 300 ms are basically removed, and that the noise at 240 ms is reduced by 10 dB. To verify the effectiveness and advantages of the VMD, the SNR and RMS error (RMSE) are calculated to evaluate the denoising performance. The SNR and RMSE are defined by (9) and (10), respectively, as follows:

$$SNR = 10\log\left(\frac{\sum_n x^2(n)}{\sum_n [x(n)-\hat{x}(n)]^2}\right) \tag{10}$$

$$RMSE = \sqrt{\frac{\sum_n [x(n)-\hat{x}(n)]^2}{N}} \tag{11}$$

Here, N represents the length of the signal, $x(n)$ denotes the standard leak signal, and $\hat{x}(n)$denotes the de-noised signal. The value of $\sum_n [x(n)-\hat{x}(n)]^2$ represents the deviation between the acquired and real signals; hence, the higher the SNR and the lower the RMSE, the better the de-noising effect.

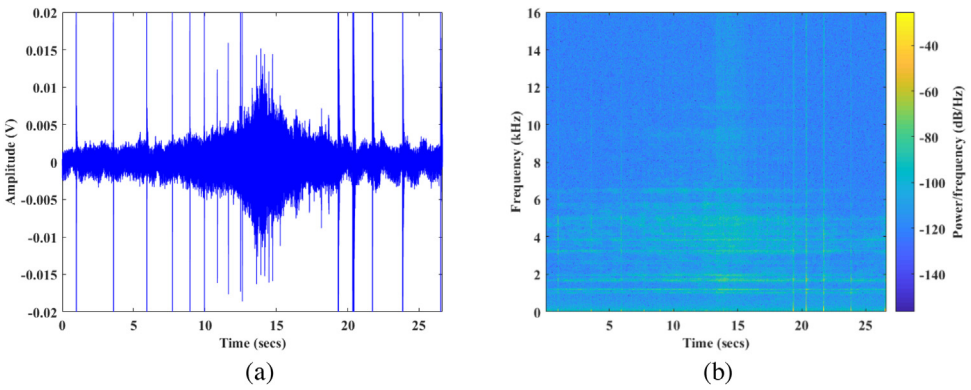

Fig. 7. (**a**) Leak signal as the SD rolls from one end to another. (**b**) Short-time Fourier transform (STFT) of the leak signal.

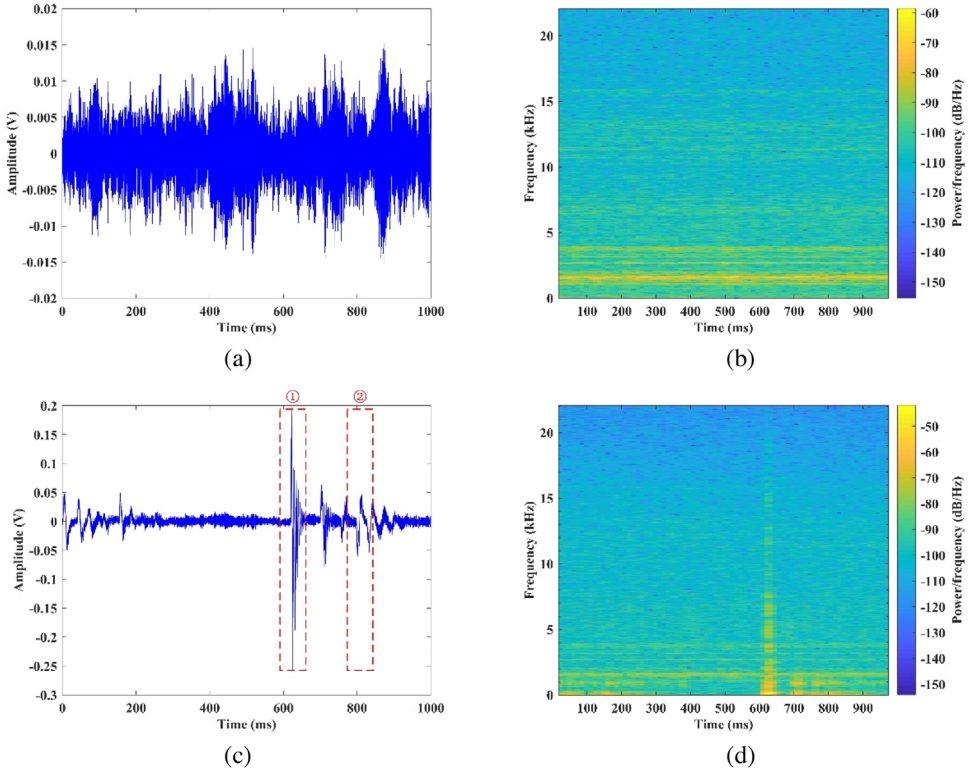

Fig. 8. (**a**) Standard leak signal measured when the SD is still. (**b**) STFT of the standard signal. (**c**) Leak signal with interference measured when the SD is rolling. (**d**) STFT of the leak signal with inference.

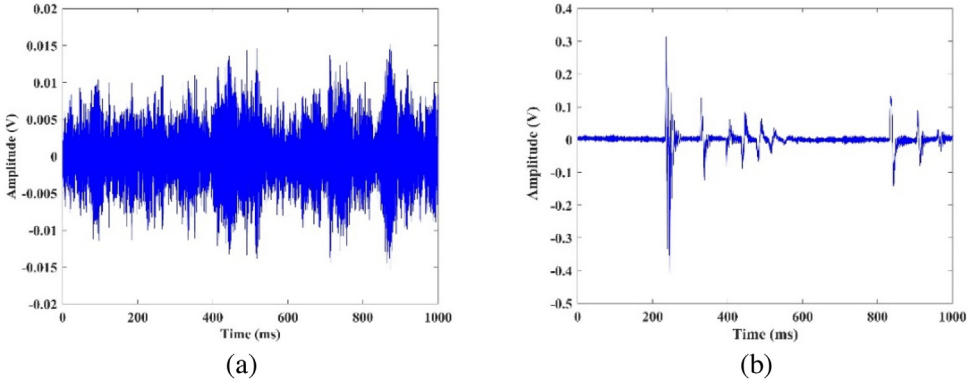

Fig. 9. (**a**) Standard leak signal used for comparison. (**b**) Synthetic signal composed of the standard leak signal and a rolling signal.

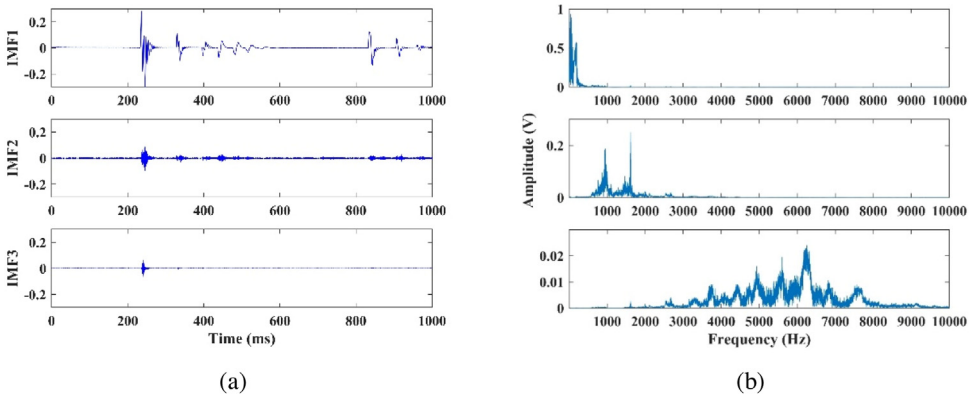

Fig. 10. (**a**) Intrinsic mode function (IMF) components of the synthetic leak signal. (**b**) Corresponding normalized frequency spectra.

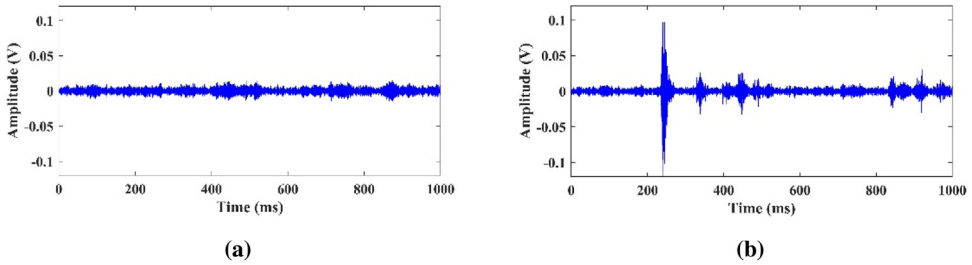

Fig. 11. (**a**) Reference leak signal. (**b**) De-noised leak signal using variational mode decomposition (VMD).

Table 3
Signal-to-noise ratio (SNR) and root mean square error (RMSE) for normal filtering and variational mode decomposition (VMD).

	Original signal	Normal Filtering	Wavelet Filtering	VMD
SNR (dB)	−16.68	0.04	1.01	1.94
RMSE	0.1026	0.0038	0.0032	0.0029

A conventional Butterworth bandpass filter and wavelet filter with a db06 wavelet basis are used for comparison. The cutoff frequencies are 600 Hz and 4000 Hz, respectively. The results are shown in Table 3. It can be seen that the VMD method has the highest SNR and lowest RMSE; that is, the VMD can effectively remove the interference noise produced by the bouncing of the SD.

5. Leak recognition using MFCCs and support vector machine (SVM)

5.1. Feature extraction

MFCCs are used to extract the features of acoustic leak signals. MFCCs have been widely applied in ASR since their publication. They depict the frequency distribution of acoustic signals based on the Mel frequency scale. Studies on the acoustic mechanisms of humans have found the existence of formants when people speak; a formant is the spectral shaping that is owing to the acoustic resonance of the human vocal tract. The spectrogram contains several formants with local maxima. Different speech signals have their own formants at different frequencies, which constitute the character of a speech signal. Identifying the formants in a spectrogram is of great importance for ASR, and MFCCs express a great ability to determine the formants between various acoustic signals.

Fig. 5 shows that the spectrum of the leak signal has similar peaks at specific frequencies, which are called the characteristic frequencies of the leak signal (Tandon, 1997). This special frequency energy distribution can be characterized by the MFCCs to distinguish leak signals from other signals. In this study, the number of MFCCs was set as 12, considering the computational complexity and recognition accuracy.

Table 4
Experiment conditions of leak.

Leak aperture (mm)	Leak rate (L/min)	Pipe pressure (MPa)	Sample number
0.4	0.30	1.0	100
0.6	0.71	1.0	100
0.8	1.74	1.0	100
1.0	2.12	1.0	100

5.2. Recognition model based on SVM

An SVM-based classifier was constructed to distinguish between leak and non-leak signals, owing to its good ability to separate the two-category data. The SVM is a supervised learning model used for classification and regression analysis. Compared with other artificial neural networks, e.g., back propagation, the SVM is not subject to many practical problems such as high dimensions, over-learning, and non-linearity. Moreover, the SVM has a good ability to deal with small samples. In this study, a specialized toolkit named LIBSVM, running on MATLAB, was applied to execute the recognition process (Chang and Lin, 2011).

Leak data with different leak apertures were collected using the experimental setup presented in Section 2. As shown in Table 4, the leak apertures were 1.0, 0.8, 0.6, and 0.4 mm. Correspondingly, the mean leak rates were 2.12 L/min, 1.74 L/min, 0.71 L/min, 0.3 L/min, respectively. The pipe pressure was maintained at 1.0 MPa. One hundred samples were collected for each condition. Otherwise, 400 samples of non-leak signals were collected as the control group. The MFCCs of all samples were extracted as the training characteristics for the SVM.

Table 5
Performance of the support vector machine (SVM) classification model.

(**a**) Recognition results of the model.

Signal type	Training set	Non-leak	1mm	0.8mm	0.6mm	0.4mm
Correct number	365/400	355/400	98/100	98/100	94/100	99/100

(**b**) Performance metric index.

TP	TN	FP	FN	Accuracy (%)	Specificity (%)
389	355	45	11	93	89.6

5.3. Results and discussion

Half of the leak and non-leak samples were randomly selected to constitute the training set. The remaining samples were denoted as the testing set. Two indicators were used to assess system performance. First, the specificity, i.e., the capability of the model to identify leaks only when they occur, was calculated as follows:

$$\text{Specificity} = \frac{\text{TP}}{\text{TP+FP}} * 100\%$$

Second, the accuracy, i.e., the capability of the model to identify leak and non-leak cases, was calculated as follows:

$$\text{Accuracy} = \frac{\text{TP+TN}}{\text{FP+FN+TP+TN}} * 100\%$$

In the above, TP represents the true positive (i.e., a correct judgment on leak cases), TN represents the true negative (a correct judgment on non-leak cases), FP represents the false positive (a wrong judgment on leak cases), and FN represents a false negative (a wrong judgment on non-leak cases).

The performance of the classification model based on the MFCCs is presented in Table 5. It can be seen that when a leak occurs, the system exhibits a rather high identification rate, as 389 of 400 samples are successfully recognized. When no leak occurs, the false alarm rate is approximately 11.25 %. The accuracy of the system is 93 %, and the specificity of the system is 89.6 %. The specificity is slightly lower than the accuracy of the model, the reason being that the false alarm rate can reach up to 11.25 %. False alarms are inevitable in both external and internal leak detection methods. One advantage of the method proposed in this work is that several SDs can be used at the time in one pipeline; therefore, the false alarm rate can be reduced, and the accuracy of the system can be further improved. In summary, the proposed SVM recognition model shows a good ability to distinguish leak signals.

6. Conclusion

This paper presents VMD-SVM combined algorithms for pipeline leak detection using an SD. A laboratory leak simulated setup for mimicking a field scenario of leak detection conducted by the SD is constructed to acquire leak acoustic signals when the SD is still or rolling. The measured data show that severe interference noises are generated by the friction and collision between the SD and pipe wall while the SD is rolling forward inside the pipeline. VMD is employed to separate the different components of the noise-contaminated leak signals and selectively reconstruct the leakage signals. Given that each IMF component is distinguished by its center frequency, the mode number K is determined based on the center frequency. The correlation coefficients between the decomposition modes and leak signal are calculated, and the modes with high correlation are selected to constitute the de-noised signal. The MSE and SNR are used to evaluate the de-noising effect. It is demonstrated that the VMD-based algorithm is capable of significantly suppressing collision-based noises. Furthermore, the MFCCs are extracted and used to constitute the characteristic vector for SVM-based leak recognition. The results show that the trained neural network can effectively identify whether a leak exists. The recognition accuracy reaches up to 93 %, and the specificity of the system is 89.6 %. In the future, additional characteristic parameters will be studied to better distinguish between the leak and interference signals, aiming to reduce the false alarm rate.

Declaration of Competing Interest

The authors report no declarations of interest.

Acknowledgments

This research was funded by National Natural Science Foundation of China (61803280, 61973227, 62001329) and Natural Science Foundation of Tianjin (JCQNJC01700).

References

Ahadi, M., Bakhtiar, M.S., 2010. Leak detection in water-filled plastic pipes through the application of tuned wavelet transforms to Acoustic Emission signals. Appl. Acoust. 71, 634–639, http://dx.doi.org/10.1016/j.apacoust.2010.02.006.

Basu, J., RoyChaudhuri, C., 2016. Graphene nanogrids FET immunosensor: signal to noise ratio enhancement. Sensors (Basel, Switzerland) 16.

Brennan, M.J., Karimi, M., Almeida, F.C.L., de Lima, F.K., Ayala, P.C., Obata, D., Paschoalini, A.T., Kessissoglou, N., 2017. On the role of vibro-acoustics in leak detection for plastic water distribution pipes. Procedia Eng. 199, 1350–1355, http://dx.doi.org/10.1016/j.proeng.2017.09.350.

Chang, C.-C., Lin, C.-J., 2011. LIBSVM: a library for support vector machines. ACM Trans. Intell. Syst. Technol. (TIST) 2, 27.

Chun-hua, T., Jun-chi, Y., Jin, H., Yu, W., Dong-Sup, K., Tongnyoul, Y., 2012. Negative pressure wave based pipeline leak detection: challenges and algorithms. In: Proceedings of 2012 IEEE International Conference on Service Operations and Logistics and Informatics, Piscataway, NJ, USA, pp. 376–380, 8–10 July.

Cui-wei, L., Yu-xing, L., Jun-tao, F., Guang-xiao, L., 2015. Experimental study on acoustic propagation-characteristics-based leak location method for natural gas pipelines. Process. Saf. Environ. Prot. 96, 43–60, http://dx.doi.org/10.1016/j.psep.2015.04.005.

Davis, S., Mermelstein, P., 1980. Comparison of parametric representations for monosyllabic word recognition in continuously spoken sentences. IEEE Trans. Acoust. Speech Signal Process. 28, 357–366.

Dragomiretskiy, K., Zosso, D., 2014. Variational mode decomposition. IEEE Trans. Signal Process. 62, 531–544, http://dx.doi.org/10.1109/TSP.2013.2288675.

Gao, Y., Brennan, M.J., Joseph, P.F., Muggleton, J.M., Hunaidi, O., 2004. A model of the correlation function of leak noise in buried plastic pipes. J. Sound Vib. 277, 133–148, http://dx.doi.org/10.1016/j.jsv.2003.08.045.

Gao, Y., Liu, Y., Muggleton, J.M., 2017. Axisymmetric fluid-dominated wave in fluid-filled plastic pipes: loading effects of surrounding elastic medium. Appl. Acoust. 116, 43–49, http://dx.doi.org/10.1016/j.apacoust.2016.09.016.

Guo, S., Chen, S., Huang, X., Zhang, Y., Jin, S., 2014. CFD and experimental investigations of drag force on spherical leak detector in pipe flows at high Reynolds number. CMES - Comput. Model. Eng. Sci. 101, 59–80.

Huang, N.E., Shen, Z., Long, S.R., Wu, M.L.C., Shih, H.H., Zheng, Q.N., Yen, N.C., Tung, C.C., Liu, H.H., 1998. The empirical mode decomposition and the Hilbert spectrum for nonlinear and non-stationary time series analysis. Proc. R. Soc. A-Math. Phys. Eng. Sci. 454, 903–995, http://dx.doi.org/10.1098/rspa.1998.0193.

Hunaidi, O., Chu, W.T., 1999. Acoustical characteristics of leak signals in plastic water distribution pipes. Appl. Acoust. 58, 235–254.

Jaesun, L., Achenbach, J.D., Younho, C., 2018. Use of the reciprocity theorem for a closed form solution of scattering of the lowest axially symmetric torsional wave mode by a defect in a pipe. Ultrasonics 84, 45–52, http://dx.doi.org/10.1016/j.ultras.2017.10.011.

Jinghui, X., Chai, K.T.C., Guoqiang, W., Beibei, H., Wai, E.L.C., Wei, L., Yeo, J., Nijhof, E., Yuandong, G., 2019. Low-cost, tiny-sized MEMS hydrophone sensor for water

pipeline leak detection. IEEE Trans. Ind. Electron. 66, 6374–6382, http://dx.doi.org/10.1109/TIE.2018.2874583.
Jingyi, D., Lichun, W., Chi, C., Cong, Y., Guoxin, Z., 2017. Study on distributed optical fiber heating pipeline network leak detection system. In: Proceedings of 2017 IEEE 2nd Information Technology, Networking, Electronic and Automation Control Conference (ITNEC), Piscataway, NJ, USA, pp. 137–140, 15–17 December.
Kumar, D., Dezhan, T., Naifu, Z., Shah, R.A., Dibo, H., Hongjian, Z., 2017a. The free-swimming device leakage detection in plastic water-filled pipes through tuning the wavelet transform to the underwater acoustic signals. Water 9, http://dx.doi.org/10.3390/w9100731, 731 (716 pp.).
Kumar, D., Tu, D.Z., Zhu, N.F., Hou, D.B., Zhang, H.J., 2017b. In-line acoustic device inspection of leakage in water distribution pipes based on wavelet and neural network. J. Sens., 10, http://dx.doi.org/10.1155/2017/5789510.
Laven, K., Mergelas, B., Inglehart, L., Larsen, M., 2006. Leak detection in large diameter fiberglass pipe. In: Proceedings of Pipelines 2006, Chicago, IL, United States, p. 31, July 30, 2006–August 2.
Li, C., Zhang, J., Zhang, Z., Hu, J., Li, Y., 2014. The research on leak detection technology of natural gas pipeline based on EMD. In: Shao, J., Zhang, Y.Q. (Eds.), Current Development of Mechanical Engineering and Energy, Pts 1 and 2, vol. 494–495, pp. 793–796.
Li, J., Zheng, Q., Qian, Z., Yang, X., 2019. A novel location algorithm for pipeline leakage based on the attenuation of negative pressure wave. Process Saf. Environ. Prot. 123, 309–316, http://dx.doi.org/10.1016/j.psep.2019.01.010.
Liu, J., Li, T., Liu, T., Li, Q., 2003. The attenuation characteristics of waves in fluid-filled pipes surrounded by elastic media. J. Huazhong Univ. Sci. Technol. 31, 90–92.
Liu, C., Li, Y., Fang, L., Xu, M., 2017. Experimental study on a de-noising system for gas and oil pipelines based on an acoustic leak detection and location method. Int. J. Press. Vessel. Pip. 151, 20–34, http://dx.doi.org/10.1016/j.ijpvp.2017.02.001.
Mengfei, Z., Zheng, P., Yunwen, L., Qiang, Z., Yijun, C., Haitian, P., 2019. Leak detection and location based on ISLMD and CNN in a pipeline. IEEE Access 7, 30457–30464, http://dx.doi.org/10.1109/ACCESS.2019.2902711.
Mostafapour, A., Davoudi, S., 2013. Analysis of leakage in high pressure pipe using acoustic emission method. Appl. Acoust. 74, 335–342, http://dx.doi.org/10.1016/j.apacoust.2012.07.012.
Muggleton, J.M., Brennan, M.J., Pinnington, R.J., 2002. Wavenumber prediction of waves in buried pipes for water leak detection. J. Sound Vib. 249, 939–954, http://dx.doi.org/10.1006/jsvi.2001.3881.
Papastefanou, A.S., Joseph, P.F., Brennan, M.J., 2012. Experimental investigation into the characteristics of in-pipe leak noise in plastic water filled pipes. Acta Acust. United Acust. 98, 847–856, http://dx.doi.org/10.3813/AAA.918568.
Sun, J.D., Wen, J.T., 2013. Target location method for pipeline pre-warning system based on HHT and time difference of arrival. Measurement 46, 2716–2725, http://dx.doi.org/10.1016/j.measurement.2013.04.059.
Tandon, K.K., 1997. MFL tool hardware for pipeline inspection. Mater. Perform. 36, 75–79.
Tang, B., Dong, S., Song, T., 2012. Method for eliminating mode mixing of empirical mode decomposition based on the revised blind source separation. Signal Process. 92, 248–258, http://dx.doi.org/10.1016/j.sigpro.2011.07.013.
Waleed, D., Mustafa, S.H., Mukhopadhyay, S., Abdel-Hafez, M.F., Jaradat, M.A.K., Dias, K.R., Arif, F., Ahmed, J.I., 2019. An in-pipe leak detection robot with a neural-network-based leak verification system. IEEE Sens. J. 19, 1153–1165, http://dx.doi.org/10.1109/JSEN.2018.2879248.
Xie, M., Tian, Z., 2018. A review on pipeline integrity management utilizing in-line inspection data. Eng. Fail. Anal. 92, 222–239, http://dx.doi.org/10.1016/j.engfailanal.2018.05.010.
Xu, Q., Zhang, L., Liang, W., 2013. Acoustic detection technology for gas pipeline leakage. Process Saf. Environ. Prot. 91, 253–261, http://dx.doi.org/10.1016/j.psep.2012.05.012.
Xu, T., Chen, S., Guo, S., Huang, X., Li, J., Zeng, Z., 2019. A small leakage detection approach for oil pipeline using an inner spherical ball. Process Saf. Environ. Prot. 124, 279–289, http://dx.doi.org/10.1016/j.psep.2018.11.009.
Zhong, J.-H., Wong, P.K., Yang, Z.-X., 2016. Simultaneous-fault diagnosis of gearboxes using probabilistic committee machine. Sensors 16, http://dx.doi.org/10.3390/s16020185.

Update

Process Safety and Environmental Protection

Volume 158, Issue , February 2022, Page 727

DOI: https://doi.org/10.1016/j.psep.2021.12.030

Process Safety and Environmental Protection 158 (2022) 727–727

Contents lists available at ScienceDirect

Process Safety and Environmental Protection

journal homepage: www.elsevier.com/locate/psep

orrigendum

Corrigendum to “Pipeline leak detection based on variational mode decomposition and support vector machine using an interior spherical detector” [Process Saf. Environ. Prot. 153 (2021) 167–177]

ianshu Xu[a,b], Zhoumo Zeng[a,b], Xinjing Huang[a,b,*], Jian Li[a,b], Hao Feng[a,b]

State Key Laboratory of Precision Measuring Technology and Instruments, Tianjin University, Tianjin 300072, China
Binhai International Advanced Structural Integrity Research Centre, Tianjin 300072, China

The authors regret that the funding reference for Natural Science oundation of Tianjin was incomplete in the published paper. The ull reference is 19JCQNJC01700.

The corrected Acknowledgements section in full is given below nd has been updated in the online version of this paper.

The authors would like to apologise for any inconvenience aused.

Acknowledgments

This research was funded by National Natural Science Foundation of China (61803280, 62073233, 62001329) and Natural Science Foundation of Tianjin (19JCQNJC01700).

DOI of original article: https://doi.org/10.1016/j.psep.2021.07.024
* Corresponding author at: State Key Laboratory of Precision Measuring Technology nd Instruments, Tianjin University, Tianjin 300072, China.
E-mail address: huangxinjing@tju.edu.cn (X. Huang).

ttps://doi.org/10.1016/j.psep.2021.12.030